

# Model surfaces for paper fibers prepared from carboxymethyl cellulose and polycations

Cassia Lux, Thomas Tilger, Ramsia Geisler, Olaf Soltwedel, and Regine von Klitzing\*

*Soft Matter at Interfaces, Department of Physics, Hochschulstraße 8, 64289 Darmstadt, Germany*

E-mail: klitzing@smi.tu-darmstadt.de

Phone: +49(0)6151-16-24506

## Abstract

For a tailored functionalization of cellulose based papers, the interaction between paper fibers and functional additives have to be understood. Planar cellulose surfaces present a suitable model system for studying the binding of additives. In this work, polyelectrolyte multilayers (PEMs) as model surfaces are prepared by alternating dip coating of the negatively charged cellulose derivate carboxymethyl cellulose and a polycation, either PDADMAC or chitosan. The varied parameters of the PEM formation are the polyelectrolyte concentrations and pH (pH=2-6). Both PEM systems exhibit an exponential growth, which reveals a high mobility of the polyelectrolytes (PEs). The pH-tunable charge density leads to PEMs with different surface topographies. QCM-D experiments reveal pronounced viscoelastic properties of the PEMs. Ellipsometry and atomic force microscopy measurements show that the strong and highly charged polycation PDADMAC leads to the formation of smooth PEMs. The weak polycation chitosan results in cellulose model surfaces with higher film thicknesses and a tunable roughness. The PEMs prepared from both polycations exhibit a high water uptake when exposed to a humid environment. The resulting PEMs are suitable water-stable but water swellable model surfaces with a controllable roughness and topography.

# Introduction

Climate change has significantly increased the demand for recyclable and tunable materials with natural origin in the last years.<sup>1</sup> A material that shows great promise in replacing plastics is cellulose based paper. In its unmodified state, paper is highly biodegradable, -compatible and recyclable.<sup>2-4</sup> The cellulose fibers forming the network of paper are stabilized by hydrogen bonds and van-der-Waals forces. When the fibers get in contact with water, their swelling leads to a partial breakage of the inter-fibre stabilizing bonds.<sup>5</sup> To make paper (more) stable towards water, it is a common procedure to use functional additives in the paper making process, which link the fibers through more stable inter-fibre connections via chemical or physical bonding.<sup>6</sup> An established method for the modification is the use of polymer resins such as amine epichlorohydrins and urea formaldehyde. These resins lead to a homo- and hetero-crosslinking of the resin and the cellulose fibers.<sup>7,8</sup> The tuning of paper cannot only lead to a higher wet-strength, but can also modify characteristics such as flexibility and dry strength.<sup>9</sup>

Planar cellulose model surfaces are a valid approach for investigating the functionalization of paper.<sup>10,11</sup> Model surfaces allow to reduce measurement errors originating in the randomness of the fiber structure and open the possibility for many analysis methods for planar interfaces.<sup>11</sup> In addition, by tuning the surface structure of the thin film, both the chemical and the physical factors of the interaction between the cellulose and a functional additive can be studied. Established methods for the preparation of model surfaces and thin films are spin-, dip-, and spray-coating and the Langmuir-Blodgett (LB) or Langmuir-Schäfer (LS) deposition methods.<sup>12</sup> A general challenge in studying paper chemistry using model surfaces based on cellulose is the preparation of the model surface itself. Cellulose is not soluble in water and in most organic solvents due to the complex structure of the fiber<sup>13,14</sup> and the hydrogen bonds of the linear high molecular weight polysaccharide.<sup>15</sup> Exceptions are two-component-solvents, such as DMA/LiCl<sup>16</sup>, and ionic liquids.<sup>17</sup> Successful dip- and spin-coating of cellulose containing thin films requires either a solution or a stable and homogeneous suspension prepared by dispersing cellulose colloids with dimensions in the

size range of few nanometers. Edgar *et al.* showed that cellulose nanocrystals in a stable aqueous suspension can be spin coated onto a substrate, resulting in a homogenous film with low roughness.<sup>18</sup> Using a cellulose solution with the aforementioned two-component solvents leads to the integration of a solid component into the thin film. Removing this component requires an additional washing step, which can alter the morphology of the model surface.<sup>12,19</sup>

In this work, cellulose model surfaces were prepared from an aqueous solution of carboxymethyl cellulose (CMC, Figure 1a) by dip-coating. Compared to cellulose, in CMC the primary hydroxy groups at the C6-atoms are partly substituted with a carboxymethyl group. The negative charge of the carboxy group allows the formation of polyelectrolyte multilayers (PEM) by alternating dip-coating of CMC and a polycation. Chitosan (CHI, Figure 1b) and Polydiallyldimethylammonium chloride (PDADMAC, Figure 1c) are used as polycations in this study. The molecular structure of the biopolymer CHI is similar to that of cellulose, as it is a  $\beta$ -1,4 linked polyamino-saccharide. It can be used to tune both the wet- and dry-strength of paper through a physical linking of the fibers, as shown by Jahan *et al.*<sup>20</sup> PDADMAC, on the other hand, is a strong synthetic polyelectrolyte (PE). The charge density of the weak PEs CMC ( $pK_a \approx 4$ ) and CHI ( $pK_a \approx 6.5$ ) are pH-dependent, while PDADMAC has a permanent positive charge.

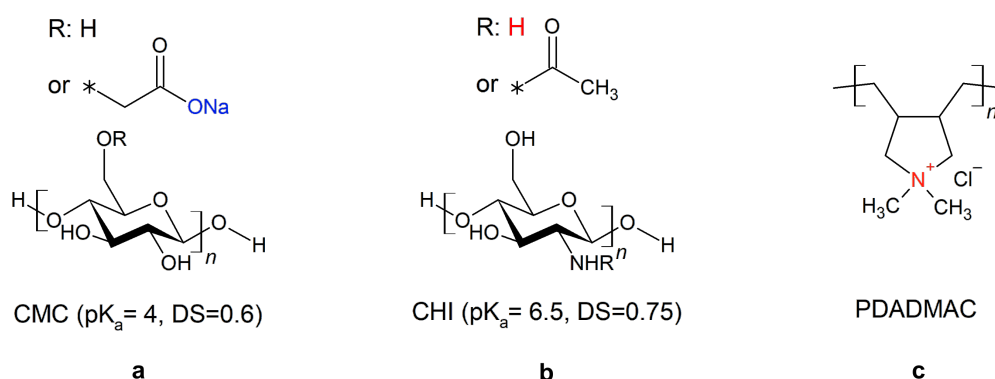


Figure 1: Chemical structures of the used PEs. The negatively charged group of CMC (a) is depicted in blue, the positive charged groups of CHI (b) and PDADMAC (c) in red. For the weak PEs the pK<sub>a</sub>-value and the degree of substitution (DS) are given.

The goal of this work is to determine the influence of the chemical composition (PDADMAC vs.

CHI) and preparation condition (pH, PE concentrations, CMC vs. polycation as outermost layer) on the morphophology and swellability of the resulting PEMs. Besides the chemical structure, PDADMAC and CHI differ in their mobility and charge density. The system CHI/CMC prepared by dip-coating was partly subject of works by the groups of Beppu *et al.*<sup>21–23</sup> and Lui *et al.*<sup>24</sup>. Beppu *et al.* determined the influence of pH-value, salt concentration and molecular weight on the formation of CMC/CHI PEMs. Contrarily to their work, the prepared PEMs in this study are mainly terminated with the CMC layer. In addition to this, the outcome of the CHI/CMC PEMs are compared to the PDADMAC/CMC PEMs and the experimental work is extended by analytical methods such as Quartz crystal microbalance with dissipation monitoring (QCM-D) and ellipsometry to study the deposition kinetics and the swellability of the PEMs. The topography of the PEMs is visualized by AFM.

## Materials and methods

### Materials

The PEs sodium carboxymethyl cellulose (CMC,  $M_W=250$  kDa, DS=0.6), polyethylenimine (PEI,  $M_W=750$  kDa, 50 wt-% in  $H_2O$ ) and chitosan (CHI,  $M_W=50-190$  kDa, DS=0.75) were purchased from Sigma Aldrich (Darmstadt, Germany). Linear polydiallyldimethylammonium chloride (PDADMAC,  $M_W=150$  kDa) was purchased from PSS (Mainz, Germany). The ammonia solution (25 %), hydrochlorid acid (1 mol/l) and sodium hydroxide solution (1 mol/l) were purchased from Merck KGaA (Darmstadt, Germany). Sulfuric acid (100%) and hydrogen peroxide (30%) were purchased from Carl Roth (Karlsruhe, Germany) and the acetic acid from VWR (Darmstadt, Germany). Ultrapure water was obtained from a Milli-Q-system from Merck with a resistance of 18 M $\Omega$  cm.



## Preparation of PEMs

The PEMs were prepared by dip-coating. As precursor, polyethylenimine was used at a concentration of  $10^{-2}$  monoM. The other PEs were dissolved in ultrapure water in the intended concentration of 1 g/l, unless stated otherwise. For a better solubility of the polycation, 0.1 M glacial acetic acid (HAc) was added to the CHI solution. For varying CHI concentration, the amount of HAc was adapted, so that the ratio of CHI and HAc remains constant (17.2 equiv. of HAc). Using hydrochloric acid and sodium hydroxide solutions (0.1 or 1 M), the pH value of all PE solutions (excluding PEI) and the rinsing water was adjusted to 4, unless stated otherwise.

Double side polished silica wafers from Siegert Wafer (Aachen, Germany) were etched in piranha solution (3:1 with  $\text{H}_2\text{SO}_4$  :  $\text{H}_2\text{O}_2$ ) for 30 min and stored in ultrapure water until used but at most for 2 h. Using a layer-by-layer dip robot (Riegler & Kirstein, Berlin, Germany), the PEMs were prepared by first adsorbing the precursor PEI for 30 min, followed by 10 min of adsorption of the polyanion CMC and 10 min of adsorption of the polycation CHI or PDADMAC. After each adsorption step, the layers were rinsed by dipping three times into rinsing water for 2 min, 1 min, and 1 min. Through alternation of the subsequent adsorption of polyanion and polycation, the PEM forms with the desired number of bilayers (NoBL). In the present work, the PEI/CMC layer is defined as the first bilayer, therefore the top layer in a bilayer is CMC.

## Ellipsometry

The measurement of the thickness and refractive index was carried out using a Null-Ellipsometer from Optrel (Sinzing, Germany) with a PCSA setup (polarizer-compensator-sample-analyzer). The wavelength of the laser was 632.8 nm, the angle of incidence was set to  $70^\circ$ . The measurements for determining the swelling ratio of the PEMs (section ) were carried out in a home-built humidity cell, which was placed in the beam path and connected to a nitrogen flow. By partly directing the nitrogen flow through two washing bottles filled with water at  $25^\circ\text{C}$ , the humidity inside the cell was controlled. The relative humidity and the temperature was measured by a thermohygrometer

from Rotronic (Ettlingen, Germany). The ratio between dried and saturated nitrogen was adjusted to reach values of the relative humidity between 0 and 95 % RH, with at least 10 steps for each measurement. After reaching a constant reading of the humidity, the PEM was left to equilibrate until no change in the ellipsometric angles was observed anymore. When preparing a PEM on a silica wafer and measuring at ambient conditions, a two-layer model is required, as described in Table 1. The  $\text{SiO}_x$  is a thin oxide layer on the substrate. As thickness of the oxide layer an average value was taken, which was determined by Löhmann *et al.*<sup>25</sup> by X-ray reflectometry.

Table 1: Summary of the parameters for the two-layer model required for the analysis of the ellipsometric data.

layer	thickness / nm	n	k
(humid) air	continuum	1.0000	0
PEM	to be fitted	to be fitted	0
$\text{SiO}_x$	1.1	1.4570	0
Si	continuum	3.8858	-0.0180

## AFM

Atomic force microscopy (AFM) was used to characterize the topography of the PEMs. The AFM measurements were carried out at ambient conditions ( $\approx 40\%$  RH) with the MFP-3D SA (Asylum Research, Oxford Instruments, California, USA). The cantilevers used are the AC160TS-R3 with a silicon probe and a tip diameter of 7-8 nm, also from Asylum Research. To determine the roughness of the PEMs,  $25\ \mu\text{m}^2$  images were taken and the roughness was determined from nine randomly selected  $1\ \mu\text{m}^2$ -areas of the image. The roughness is defined as the root mean square (RMS) of height deviations of the surface mean plane. For PEMs with surface patterns with a correlation length in the  $\mu\text{m}$  range, the roughness was determined on the whole  $25\ \mu\text{m}^2$  area. In all cases, the two different roughness measurements ( $1\ \mu\text{m}^2$ ,  $25\ \mu\text{m}^2$ ) lead to similar values.

## QCM-D

The adsorption kinetics of the PEM formation process is carried out in-situ by QCM-D measurements (QCM with dissipation monitoring Q-Sense Explorer, Biolin Scientific, Gothenburg, Sweden). The used crystals, coated with  $\text{SiO}_2$  and with a resonance frequency of 4.95 MHz, were also purchased from Biolin Scientific. Prior to the measurement, the crystals were cleaned in an ultrasonic bath with chloroform, isopropanol and water, each for 15 min and etched using the RCA procedure (5:1:1 of water: $\text{NH}_3$ : $\text{H}_2\text{O}_2$  at 75 °C for 20 min). The baseline was recorded with the rinsing solution, the dipping order of the PE solutions was the same as in the corresponding dip-coating procedure. The time of adsorption and rinsing for each layer was the time until the frequency reaches a steady state. The evaluation of the results was only done on the basis of the change in frequency and dissipation. The decrease in frequency is correlated with an increase in mass. An increase in dissipation indicates softening of the film. Comparing the different overtones of the signal gives additional information about the viscoelasticity of the thin film. Diverging overtones hint to a flexible and soft film.

## Results

First, the PEMs are characterized in dependence of the preparation parameters NoBL, pH-value and PE concentration. In addition, in-situ QCM-D measurements are carried out and the change in frequency and dissipation is determined. Afterwards, the swellability of PEMs is determined in dependence of the varied parameters by measuring the change in thickness and refractive index with varying relative humidity.

### PEM formation

PEMs prepared from the polycations PDADMAC and CHI (pH=4;  $c_{PE}=1$  g/l) with a varying NoBL are characterized with respect to their thickness and morphology by ellipsometry (Figure 2 a-b) and AFM (Figure 2 c-i), respectively. In the figure, integers correspond to a bilayer termi-

nating with the polyanion CMC and half numbers to the polycation as the outermost layer. The film thickness of both PE systems grows exponentially, whereas the CHI/CMC system results in slightly larger film thicknesses (Figure 2a). The refractive index grows with increasing film thickness and NoBL, with the exception at 3 BL, at which a much larger value is obtained (Figure 2b). In contrast, the PDADMAC/CMC system shows a significant increase in the refractive index with increasing NoBL. At 6 BL, a plateau is reached leading to a constant value at higher BL. At 9 BL, the refractive indices of both PE systems are similar to each other. A refractive index above 1.6 is uncommon for PEMs, but will be discussed later in section .

AFM measurements were carried out to determine the topography and the surface roughness of the PEMs. For selected NoBL, AFM images of PDADMAC/CMC and CHI/CMC are shown in Figures 2d-i. In the case of PDADMAC/CMC at 3 BL (Figure 2d) an overall homogeneous PEM is obtained, which contains agglomerates in the size of few tens of nanometers. At 5 BL (Figure 2e), a pronounced domain formation is observed, and at 7 BL (Figure 2f), a closed and homogeneous film is obtained. The comparison of the measured thickness and the height scale of the topography shows that the sample surface at 5 BL is not completely covered by PEM. The roughness (Figure 2c) exhibits a maximum at 5.5 BL and then reaches a constant low value in the subnanometer range for PDADMAC/CMC. The comparison of the PEMs PDADMAC/CMC (Figure 2d) and CHI/CMC (Figure 2g) at 3 BL reveals that in both cases a homogenous surface is obtained, in the sense that there are no large agglomerates. With an increasing number of adsorbed bilayers, the surface roughness of CHI/CMC increases while the surface stays macroscopically homogeneous. Beyond 6 BL, CHI/CMC exhibits a significantly higher roughness than PDADMAC/CMC.

## Adsorption kinetics

To gain further insight into the adsorption behavior and to resolve the adsorption kinetics of the PEs, in-situ QCM-D measurements were carried out. Figure 3 shows the change in frequency and dissipation for PDADMAC/CMC and CHI/CMC. To facilitate the interpretation of the data, the

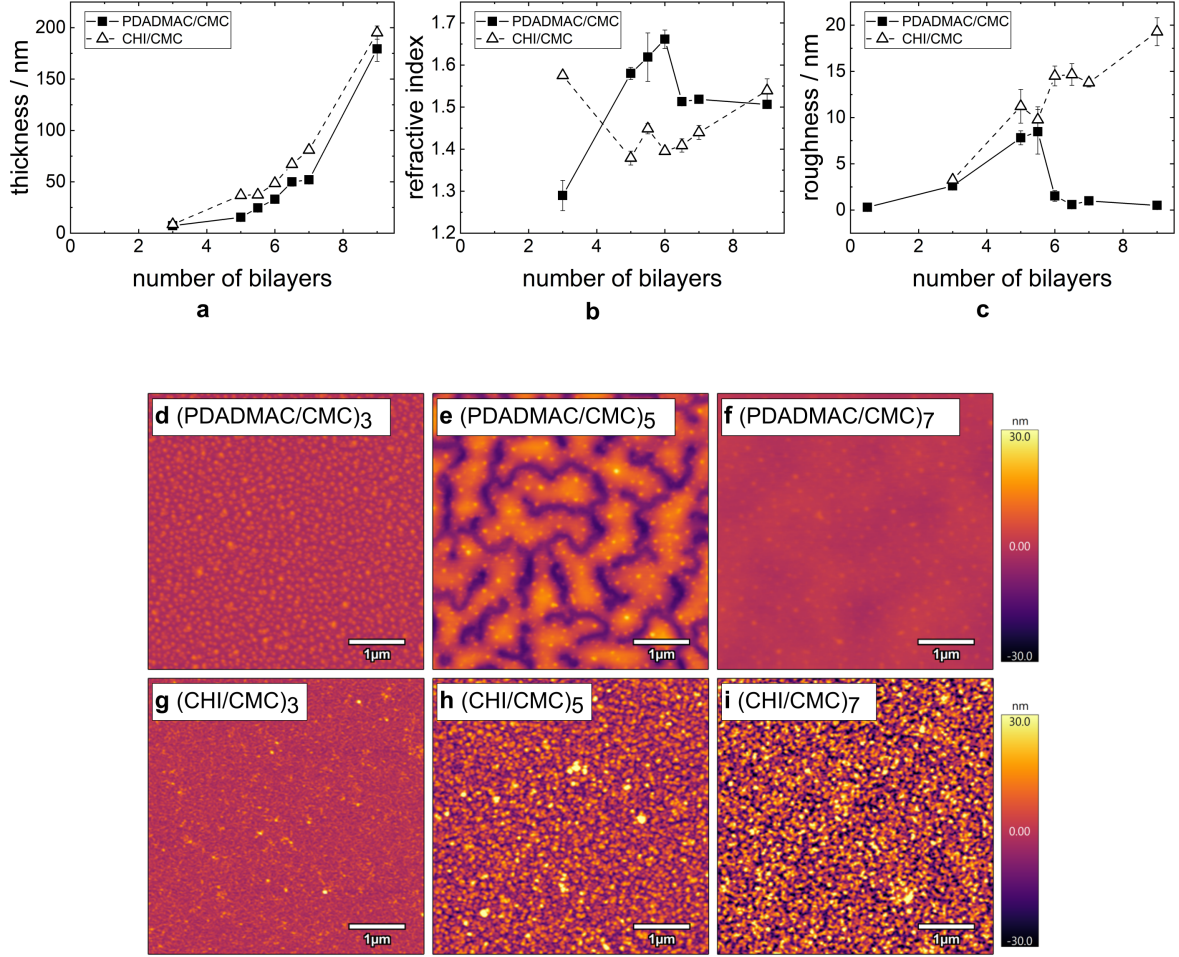


Figure 2: Summary of the morphology results for PEMS PDADMAC/CMC (filled squares) and CHI/CMC (empty triangles) from ellipsometry (a-b) and AFM measurements(c-i): (a) Film thickness, (b) refractive index and (c) roughness with an increasing NoBL. (d)-(i): AFM Images ( $5 \times 5 \mu\text{m}^2$ ) for PDADMAC/CMC and CHI/CMC at 3, 5, and 7 BL. For all images the height scale is set to 60 nm. The samples were prepared at pH 4 and  $c_{PE}=1 \text{ g/l}$ . All experiments were carried out at  $\text{RH} \approx 40\%$ . The first bilayer corresponds to the bilayer of the precoat PEI and CMC.

adsorption time periods are highlighted by different colors: gray for the adsorption of the polycation, blue for the polyanion, white for the rinsing steps. The first area corresponds to the adsorption of the precursor layer PEI. Each adsorption step was carried out until the steady state is reached so that different adsorption times result. In the adsorption experiments of both PE systems, the overall frequency decreases, while the dissipation increases. The different overtones diverge with increasing NoBL. Each adsorption step can clearly be distinguished, as the contact of the charged layer with the PE solution induces an immediate change in frequency and dissipation. The time and the progress of frequency and dissipation until the steady state is reached varies for the two PEMs and for the different PEs in one system. It can also be observed that the amount of adsorbed mass and the time until steady state generally increases with each bilayer. The rinsing steps lead at most to a small amount of desorption and a small decrease in dissipation.

Figure 3a shows an increase in mass for each of the adsorption steps of CMC in the PDADMAC/CMC PEM system. The dissipation first increases significantly and then reaches a steady state value (Figure 3c). The adsorption of CMC on the CHI layers follows a similar behavior in the first adsorption steps for the change in frequency and dissipation. For higher NoBLs, the change in dissipation during the adsorption of CMC exhibits a sharp decrease after the initial increase (Figure 3d). The adsorption of CMC has a slightly higher impact on the change of both the frequency and the dissipation on the PDADMAC/CMC PEM than on the CHI/CMC PEM. The adsorption behavior of PDADMAC in the PDADMAC/CMC PEM differs noticeably from the expected growth behavior for the first layers. Both, the frequency and the dissipation decrease during adsorption. At a higher NoBL, the adsorption returns to the expected decrease in frequency and increase in dissipation. The adsorption of CHI in the CHI/CMC PEM also shows an increase in frequency and decrease in dissipation throughout each of the adsorption steps.

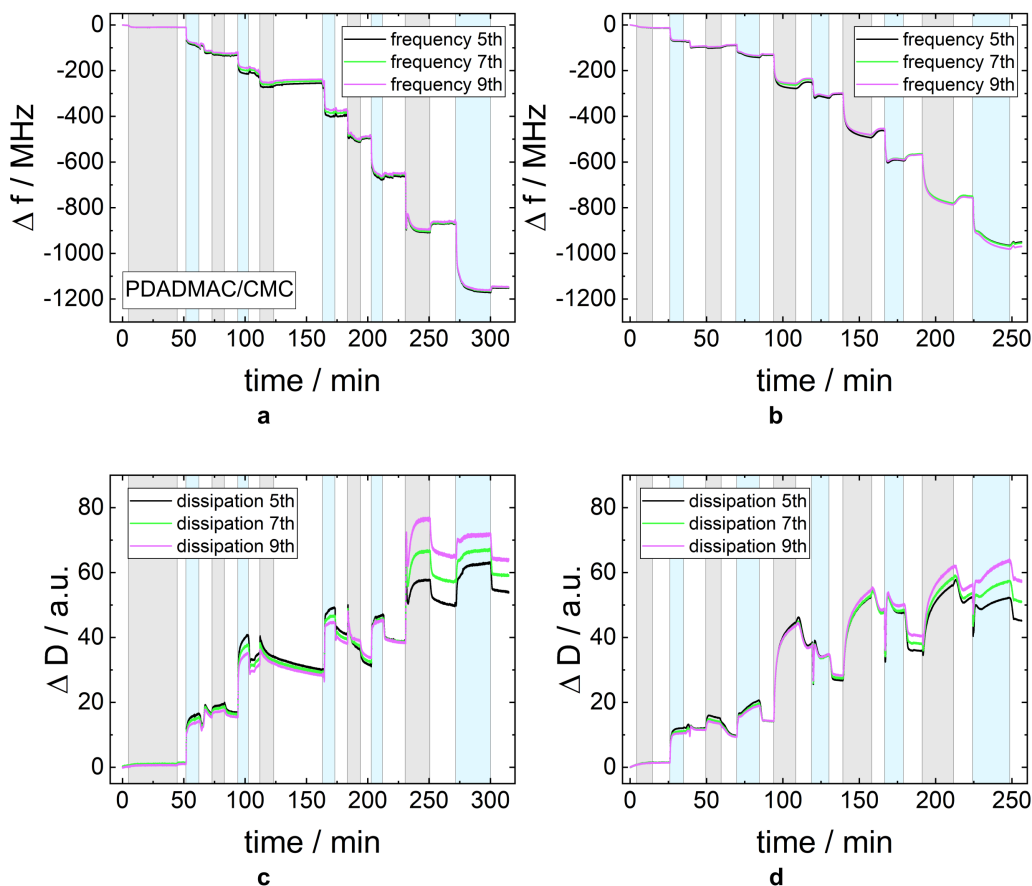


Figure 3: The change in frequency  $\Delta f$  (a-b) and dissipation  $\Delta D$  (c-d) measured by QCM-D for the PEMs PDADMAC/CMC and CHI/CMC. The gray region is the time period in which the polycation is adsorbed and the blue region in which the polyanion is adsorbed. The different curves in one plot represent the different overtones of the measured signal (5<sup>th</sup>, 7<sup>th</sup>, and 9<sup>th</sup>). All PE concentration were set to 1 g/l and the pH-value was maintained at pH=4.

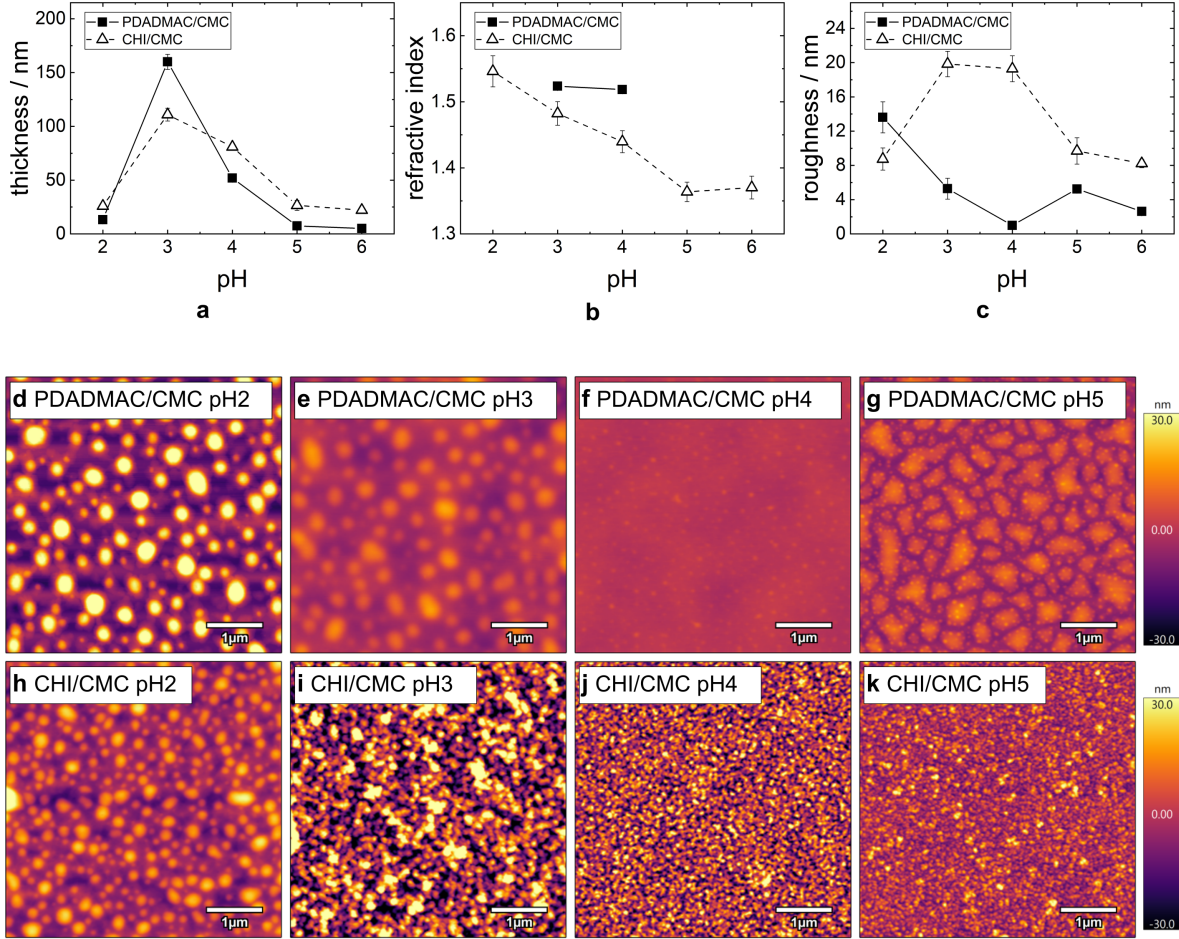


Figure 4: Summary of the morphology results for PEMS PDADMAC/CMC (filled squares) and CHI/CMC (empty triangles) from ellipsometry (a-b) and AFM measurements(c-i): (a) Film thickness, (b) refractive index and (c) roughness with varying pH-values. (d)-(i): AFM Images ( $5 \times 5 \mu\text{m}^2$ ) for PDADMAC/CMC and CHI/CMC at pH=2, 3, 4 and 5. For all images the height scale is set to 60 nm. The samples were prepared at  $c_{PE}=1 \text{ g/l}$  and 7 BL. All experiments were carried out at  $\text{RH} \approx 40\%$ .



## Influence of pH-value

The respective thicknesses and refractive indices measured by ellipsometry for the PEMs (7 BL;  $c_{PE}=1$  g/l) are shown in Figure 4. Both, PDADMAC/CMC and CHI/CMC PEMs, exhibit maximum film thickness of the film at pH 3 (Figure 4a). At pH 3, the film thickness of the PDADMAC/CMC PEM is larger than that for the CHI/CMC PEM, which is in contrast to all other pH-values. The refractive index decreases with increasing pH-values for the CHI/CMC PEM, reaching a constant value at about pH 5 (Figure 4b). For PDADMAC/CMC, only the refractive indices for pH 3 and pH 4 are shown. Due to the small film thickness, the fitting of independent parameters (thickness and refractive index) was not reliable for the other pH-values. Nevertheless, it can be observed that the refractive indices of the PEMs at pH=3 and pH=4 for PDADMAC/CMC are similar.

The topography of PDADMAC/CMC and CHI/CMC PEMs in dependence of the pH and at 7 BL was studied by AFM (Figure 4d-k). Height images reveal for both PE systems a strong agglomeration at pH 2 (Figure 4d and h). The agglomerates are spherical and have lateral diameters of several hundreds of nanometers. As can be seen from the height and lateral scale, PDADMAC/CMC leads to larger agglomerates in all dimensions but a lower packing density compared to the CHI/CMC PEM. With increasing pH, the PDADMAC/CMC agglomerates decrease in size and the PEMs are overall smoother. The spherical aggregation progresses into a domain formation (Figure 4g). Figure 4c confirms the maximum roughness for pH 2 for PDADMAC/CMC and the smoothest PEM with the lowest roughness is obtained at pH 4. This is in agreement with the topography images, as large agglomerates correlate with a high roughness. For the CHI/CMC PEM the aggregate size decreases and a higher packing density with increasing pH-value is obtained (Figure 4h-k). Here, the CHI/CMC PEMs have the largest roughness at pH 3 and pH 4 (Figure 4c). Overall, the roughness is generally lower for the PDADMAC/CMC PEMs compared to the CHI/CMC PEMs.

## **Influence of PE concentration**

In the following, the influence of the PE concentration (0.1-5 g/l) on the thin film morphology is investigated. The respective morphology results of the prepared PEMs PDADMAC/CMC and CHI/CMC (7 BL; pH=4) are summarized in Figure 5 as function of the PE concentration. While the thickness of the PDADMAC/CMC PEMs is largest at a PE concentration of 1 g/l, the thickness of the CHI/CMC PEMs linearly increases with the PE concentration within error bars (Figure 5a). For this system, the refractive index also increases with a rising PE concentration (Figure 5b). For PDADMAC/CMC PEMs, the refractive index could only be determined for the thickest film prepared at 1 g/l.

The PEM topography with varying PE concentration measured by AFM is shown in Figures 5d-i. The PDADMAC/CMC PEMs prepared at 0.1 and 5 g/l shows a dewetting (Figures 5d and f), while the PEM at 1 g/l is rather homogeneous (Figure 5e). The domain formation at 0.1 g/l is more prominent than for 5 g/l and might lead to incomplete coverage. In agreement with the topography, the roughness for this system is lowest at 1 g/l and highest at 0.1 g/l. The surface of the CHI/CMC PEMs is more inhomogeneous of the PEMs prepared at 0.1 g/l (Figure 5g) and 5 g/l (Figure 5i) compared to the PEM prepared at 1 g/l (Figure 5h). The roughness decreases slightly with increasing concentration, which is in agreement with the topography images. Overall, the roughness of all CHI/CMC PEMs is significantly higher compared to the roughness of the PDADMAC/CMC PEMs.

Since the low thickness of the PDADMAC/CMC PEM at 5 g/l (Figure 5a) was unexpected, the layer formation was additionally studied by QCM-D experiments (Figure 6). As the higher viscosity of the PE solutions impacts the shearing of the quartz crystal, a quantitative comparison between the different PE concentrations can only be done for the rinsing periods (Figure 6, white regions). The frequency change of the different rinsing periods shows a rather linear (instead of exponential) growth of the PEM. The decrease in frequency during the adsorption periods of CMC

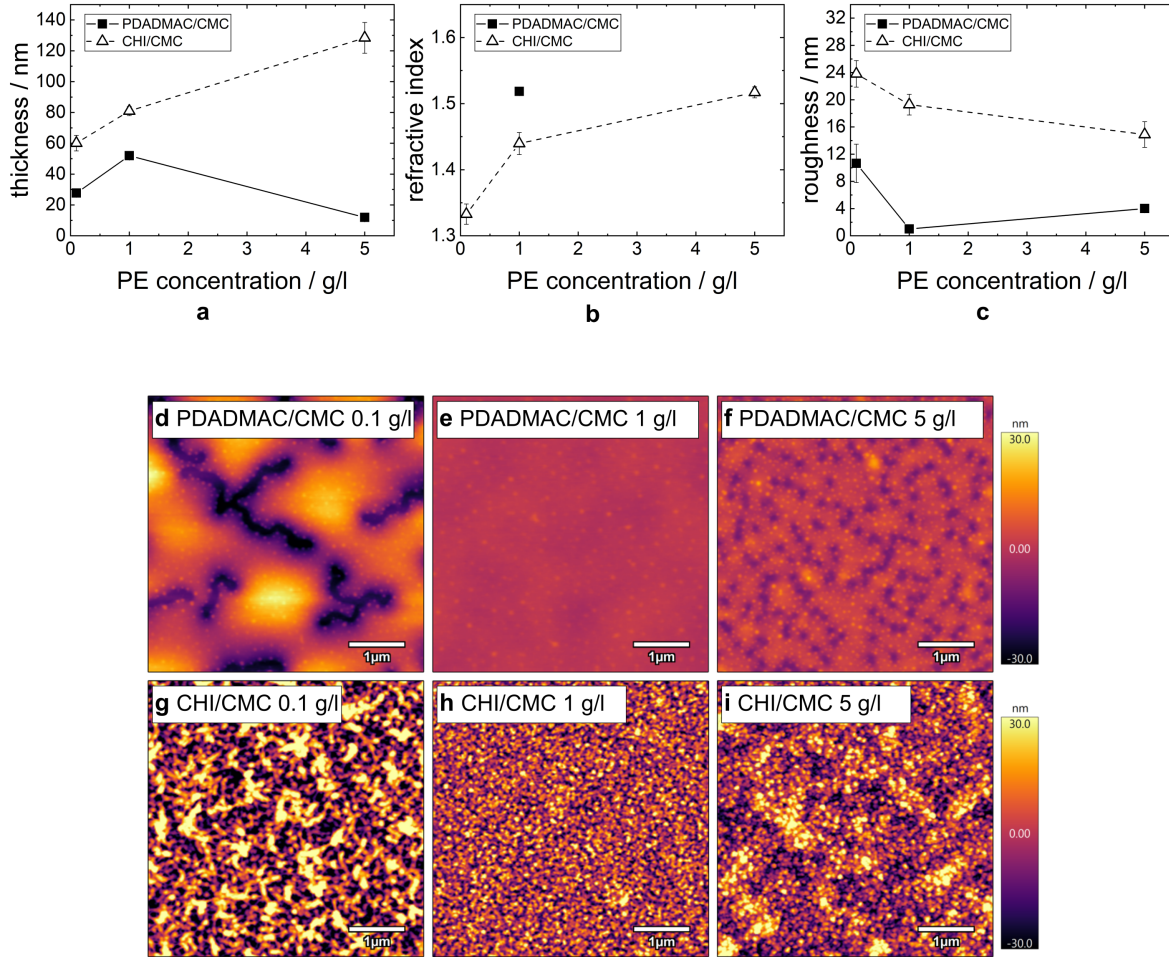


Figure 5: (a) and (b): Change in thickness and refractive index for PDADMAC/CMC (filled squares) and CHI/CMC (empty triangles) with varying PE concentration determined by ellipsometry ( $RH \approx 40\%$ ). (c): Change in roughness, determined by AFM ( $RH \approx 40\%$ ), with varying PE concentration. for PDADMAC/CMC (filled squares) and CHI/CMC (empty triangles). (d)-(i): AFM Images ( $5 \times 5 \mu\text{m}^2$ ) for PDADMAC/CMC and CHI/CMC varying PE concentration. For all images the height scale is set to 60 nm. The NoBL was set to 7 and the concentration of all solutions was set to 1 g/l. The first bilayer corresponds to the bilayer of the precoat PEI and CMC.

shows an increase in adsorbed mass (Figure 6a, blue regions). In contrast to this, the adsorption of PDADMAC (Figure 6a, gray regions) leads to an initial increase in adsorbed mass, followed by slow increase in frequency, thus a desorption. The rinsing process after each PDADMAC adsorption step results in a final frequency equal to the frequency prior of the adsorption step. This means that the adsorption and rinsing of PDADMAC has no impact on the overall change in frequency for this layer and with that on the total adsorbed mass on the substrate. In addition, the resulting frequency change is significantly lower than for the PEMs prepared at 1 g/l (Figure 3a and c). Figure 6b shows that the film viscoelastic properties do not change significantly, as the dissipation only increases by a much slower rate, if at all, compared to the previously studied systems (Figure 3b and d). The relatively stronger spreading of the overtones with respect to the overall dissipation during the adsorption steps is most likely an impact of the higher viscosity of the 5 g/l. The results of the measurement with the QCM-D are in good agreement with the observed inhibited growth of the PDADMAC/CMC PEM prepared at 5 g/l (Figure 5a).

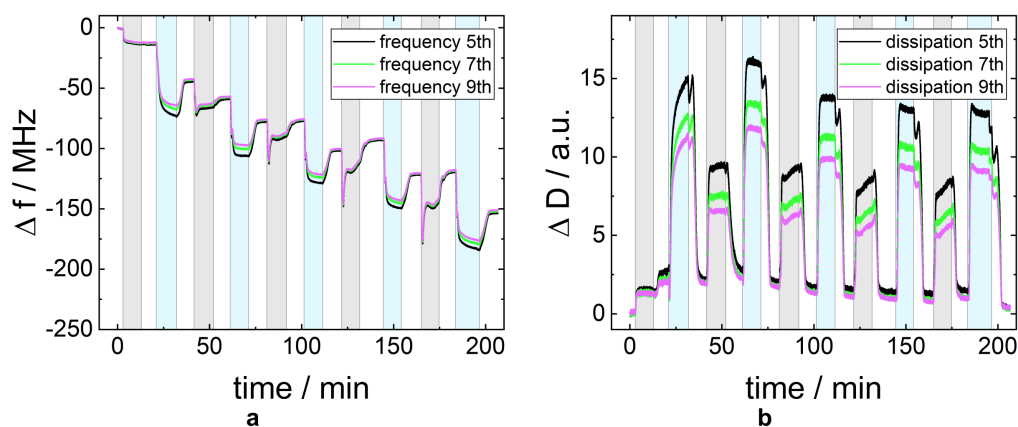


Figure 6: The change in frequency  $\Delta f$  (a) and dissipation  $\Delta D$  (b) measured by QCM-D for the PEM PDADMAC/CMC at 5 g/l. The gray region is the time period in which the polycation is adsorbed, the blue region in which the polyanion is adsorbed and white for the rinsing periods. The different curves in one plot represent the different overtones of the measured signal ( 5<sup>th</sup>, 7<sup>th</sup>, and 9<sup>th</sup>). The pH-value was maintained at pH=4.

## Swelling of PEM

PEMs are responsive materials, which respond to the surrounding relative humidity with a thickness change of the thin film. The swelling behavior of the PEMs is studied by measuring the thickness with ellipsometry at varying relative humidity (0 - 90% RH). Through the increase of the relative humidity in the measuring chamber, the water content inside the PEM increases, leading to a swelling of the PEM. The swelling coefficient  $S$  (Equation 1) being a measure for the water content, is calculated from the difference in thickness  $d$  and the thickness of the dry PEM  $d_0$  (1% RH).

$$S = \frac{d - d_0}{d_0}. \quad (1)$$

Figure 7 shows the swelling coefficient as a function of RH for both investigated PE systems. With increasing humidity the film thicknesses of the studied PEMs PDADMAC/CMC and CHI/CMC increases (Figure 7a). Nevertheless, a different swelling behavior is observed for the two PE systems. The PDADMAC/CMC PEMs first swell linearly up to 70% RH. Above 70% RH, the film thickness swells exponentially. In addition, the water uptake depends on the outermost PE layer (polycation or polyanion). As shown in figure 7, the progression of the curves for the PEMs with CMC as the outermost layer (6 BL and 7 BL) is identical. For the PEM with PDADMAC as outermost layer (6.5 BL) a higher water uptake is observed. In the case of CHI/CMC, the swelling coefficient increases linearly with the relative humidity and is independent of the outermost PE. When comparing both PE systems to each other, it can be seen that the PDADMAC/CMC PEMs have overall higher swelling ratios, thus incorporate a higher quantity of water than the CHI/CMC PEMs.

The swelling behavior was also studied for PEMs prepared at different pH-values, as the charge density most likely has a structural effect on the thin film. Figure 7b shows the swelling coefficient in dependence of the relative humidity and pH. The PDADMAC/CMC PEMs swell in a similar manner for all pH-values (3, 4 and 5). The CHI/CMC PEMs at pH 4 and 5 show a similar linear

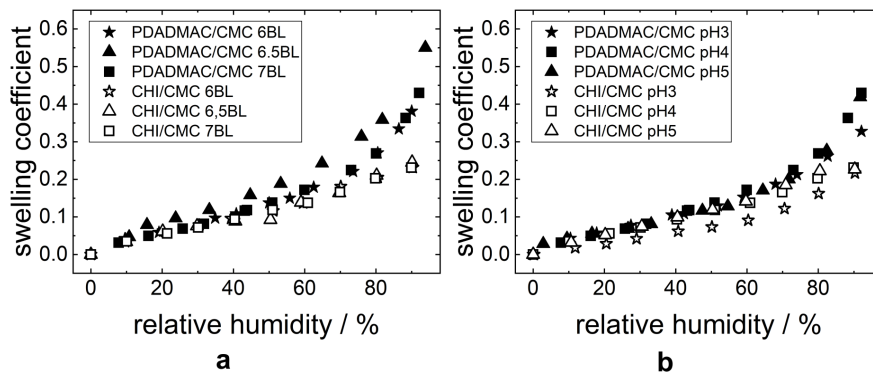


Figure 7: The swelling coefficient  $S$  in dependence of the relative humidity RH of the PEMs PDADMAC/CMC and CHI/CMC with (a) varying NoBL (at pH=4) and (b) different pH-values (7 BL). The thicknesses were measured by ellipsometry.

swelling behavior compared to the PEMs presented in Figure 7a. The swelling behavior of the thin film prepared at pH 3 is lower than for the PEMs prepared at pH 4 and 5. An exponential upturn at around 70% RH leads to superposition with the PEMs prepared at pH 4 and 5.

## Discussion

This work compares the influence of PE concentration, pH and the NoBL on PEM formation composed of varying polycations (PDADMAC or CHI) and the polyanion (CMC) with respect to the layer formation properties and surface topography characteristics. In addition, the swelling behavior at varying relative humidity is demonstrated for exemplary samples with a varying NoBL and different pH. The main analytical methods are AFM, ellipsometry and QCM-D experiments. In the following, first, the PEM formation process and the surface morphology are discussed. Next, the influence of the structure on the swellability of the PEMs is elaborated.

## Multilayer formation

Both PE systems (PDADMAC/CMC and CHI/CMC) grow exponentially with an increasing NoBL (Figures 2a, 3a and 3c). An exponential thickness growth of the PEM is linked to a high mobility of the PEs.<sup>26</sup> The mobility of the PEs determines the ability for diffusion between the bulk

PEM and the solvent. For example, PEs with a high charge density and no added salt, as is the case for PDADMAC (Figure 1c), do not diffuse into the PEM. Systems with immobile PEs, for example PDADMAC/PSS, leads to a linear thickness increase for each adsorption step.<sup>27,28</sup> From that it is concluded that the exponential growth observed for the PDADMAC/CMC PEM results from a high mobility of CMC (Figure 1a). In the CHI/CMC system both PEs are mobile enough in order to diffuse in the PEM. While, the high mobility of CMC is deduced from the thickness results of the PDADMAC/CMC system, the mobility of CHI is already confirmed in literature for the PE system Hyaluronan/CHI.<sup>29</sup> Since the high mobility of the PE contributes to the thickness growth, it is expected that the mobile and coiled CHI (Figure 1b) contributes by a higher fraction to the thickness growth compared to the immobile and rather rigid PDADMAC molecules. This in turn means that the similar layer thicknesses (Figure 2a and 3a,c) for both PE systems point to a synergistic effect of PDADMAC and CMC contributing to the large resulting thickness of the film. During the adsorption step of PDADMAC, CMC is assumed to diffuse out of the PEM bulk to the surface leading to an intrinsic charge compensation.<sup>26,28,30,31</sup> This charge compensation in turn leads to a further PDADMAC adsorption. The pronounced adsorbed amount of PDADMAC is supported by a pronounced change in frequency (Figure 3a). Since PDADMAC is the more rigid than CMC a pronounced decrease in dissipation occurs at the same time. The complexation of CMC and PDADMAC at the PEM surface and the release of counter ions leads to a denser layer and reduced layer softness (or dissipation).<sup>32</sup>

The results of the pH variation on the PEM morphology is related to the PEM structure depending on the charge density of the PE (Figure 4). On the one hand, a high charge density correlates with a slower PE diffusion and the adsorption of the stretched chains contributes less to the film thickness. On the other hand, a too low charge density can inhibit the formation of the PEMs. This is due to a lacking change in surface charge during the alternating adsorption of polycation and -anion.<sup>33,34</sup> This becomes visible in the ellipsometry measurements (Figure 4a). PDADMAC is a strong PE carrying one permanent and pH-independent charge on each monomer (Figure 1c).

CMC is a weak PE (Figure 1a,  $DS=0.6$ ,  $pK_a \approx 4$ ), whose charge density varies with the protonation state and thus with the pH of the PE solution. At low pH-values, the charge density of CMC is very low due to protonation of the carboxylic group. This results in an inhibited PEM assembly, lower film thicknesses (Figure 4a) and higher agglomeration (Figure 4c). At pH 5 and 6, the higher charge density leads to stretched chain conformation and small film thicknesses of the PEMs. At a pH-value between 3 and 4, a balance between the charge density and the coiling of the chains exists, resulting in the observed maximum film thickness (Figure 4a). The effect of the PE solution pH on the film thickness is similar for the CHI/CMC as for the PDADMAC/CMC PEMs. This trend confirms the major effect of CMC on the pH-dependency of the PEMs. The charge density of CHI ( $DS=0.75$ ,  $pK_a \approx 6.5$ ) does not vary between pH 2 and 6 due to almost complete protonation over the entire pH range. A pH-dependent effect of CHI is therefore not expected (see also Zhang et al.<sup>24</sup>) and was not observed during the experiments. At pH 3, a significantly higher film thickness is obtained for the PDADMAC/CMC PEM compared to the CHI/CMC PEM (Figure 4a) due to the higher charge density of PDADMAC than for CHI. Here, it is assumed that the mobility of the weakly charged CMC is further enhanced by PDADMAC than by CHI and a higher amount of PDADMAC is adsorbed.

The effect of the PE concentration of the dipping solutions is shown in Figures 5 and 6. The formation of PEMs is strongly controlled by the adsorption rate of the PE to the surface of the PEM. Therefore, a decrease in PE concentration influences the amount of adsorbed PE.<sup>33</sup> If the PE concentration is decreased but the adsorption time is maintained constant at 10 min, a reduced film thickness is expected.<sup>35–37</sup> This effect is confirmed for both PEM systems PDADMAC/CMC and CHI/CMC (Figure 5a). Here, the lowest PE concentration leads to the thinnest PEMs in both cases. The higher roughness observed (Figure 5c) may result from an insufficient surface coverage. As expected, an increasing PE concentration leads to a higher film thickness of the resulting PEMs (Figure 5a). For PDADMAC/CMC, the PEM formation is not monotonous since a stripping of PE complexes leads to a partial desorption (Figures 5a and 6). This effect was already observed by



Sui *et al.*<sup>38</sup> and is confirmed by the results of this study.

## Structure and Swellability

In the manuscript, it is demonstrated that the structure and morphology of the PEMs strongly depend on the preparation conditions such as NoBL, pH, and PE concentration of the dipping solution. The domain formation shown in the AFM images (Figures 2d-f) is assumed to result from a lateral agglomeration during the drying of the PEM rather than by the rinsing steps<sup>39,40</sup>. The formation of large domains explains the high refractive indices (Figure 2b) and roughness (Figure 2c) of the intermediate NoBL. The high roughness and its potential influence on the optical fitting of the ellipsometric data can lead to an underestimated film thickness and overestimated refractive index.<sup>41,42</sup> The dewetting of the PDADMAC/CMC PEMs hints to a flexible thin film. This is further supported by the low local roughness (Figure 2c, after 6 BL), which is independent of the NoBL. A roughness is independent of the film thickness when the PEMs are flexible enough to decrease interfacial tensions, thus the roughness of the PEM, or for PEM systems with highly mobile PEs diffusing into the layer.<sup>40</sup> The high flexibility of the PDADMAC/CMC complexes facilitates its high water uptake (Figure 7a). The PDADMAC terminated PEM (Figure 7a, 6.5 BL) shows a higher water uptake because of a higher concentration of counter ions<sup>43</sup> and therefore a higher osmotic pressure in the PEM.<sup>25,44</sup> This dependency of the water uptake on the outermost PE layer is commonly observed for PEMs and known as the odd-even effect.<sup>32,44–47</sup>

The CHI/CMC system does not result in observable flexible PEMs. On the one hand, Figure 2c shows an increasing roughness with increasing NoBL, as commonly observed for PEMs.<sup>48</sup> This observation and the overall higher roughness compared to PDADMAC/CMC PEM indicates that the flexibility of the CHI/CMC PEM is not high enough in order to reduce interfacial tensions through a smoothing of the surface. On the other hand, the lower flexibility reduces the water uptake of the CHI/CMC PEMs (Figure 7). The overall lower water uptake of the CHI/CMC PEMs is assumed to result from a lower concentration of counter ions. Moreover, no prominent odd-even

effect is observed since similar swelling coefficients are obtained for the PEM with CHI and with CMC as outermost layer. However, the water uptake at pH 3 is lower compared to the PEMs prepared at the higher pH-values and increases exponentially above 60 % RH. The strong chain coiling and low charge density of CMC at pH 3 seems to lead to a denser film with less counter ions present in the film. The non-linear behavior beyond 60 % RH may result from an enhanced flexibility of the film at high humidity and the release of counter ions in the polymer coils. In conclusion, the higher flexibility of the PDADMAC/CMC PEMs is assumed to result from a higher concentration of counter ions generally present in the PEM. On the one hand, the higher concentration of counter ions presumably stems from a higher extrinsic charge compensation caused by the highly charged PDADMAC. On the other hand, the high mobility of CMC and CHI leads to a complexation of the two PEs and a decrease in counter ion concentration.

## Conclusion

In this work, thin films in the form of PEMs are prepared by alternating dip-coating of the cellulose derivate CMC and the positively charged polyelectrolytes PDADMAC or CHI. These PEMs enable the study of the interaction between cellulose fibers with functional additives used for the modification of paper products. By using the cellulose derivate CMC, the water insolubility of cellulose is overcome and the formation of PEMs enabled. These PEMs exhibit unique film properties such as a controllable thickness and surface topography, which were characterized with a broad variety of experimental methods. The study reveals that PEMs formed with PDADMAC and CMC are flexible thin films. The PEMs prepared with more than 6 BL have a low roughness and show a homogeneous surface topography, which can be related to highly charged PDADMAC chains, which are adsorbed in a more stretched conformation than the CMC chains. Figure 8 shows a proposed structure for both PEM systems. Due to the high charge density, PDADMAC (Figure 8, left) has a longer effective persistence length (includes backbone rigidity and charge effects) than CMC and

CHI. Therefore, 1:1 stoichiometric complexation between PDADMAC and CMC is not fulfilled, which leads to pronounced extrinsic charge compensation by non-adsorbed counter ions in the PEM. The high amount of counter ions leads to a high osmotic pressure and a high water uptake of the PDADMAC/CMC PEMs. In addition, a lower amount of complexation sites allows parts of the PEM to move which might explain the ability to form lateral domains under certain conditions. The similarity of persistence lengths of CHI and CMC (originating from similar backbone and charge densities) leads mainly to intrinsic charge compensation and a low osmotic pressure of the CHI/CMC PEM (Figure 8, right). Since both polysaccharides have bulky monomers they form quite large loops leading to larger agglomerates (roughness) and thickness than the PDADMAC / CMC PEM under certain pH conditions.

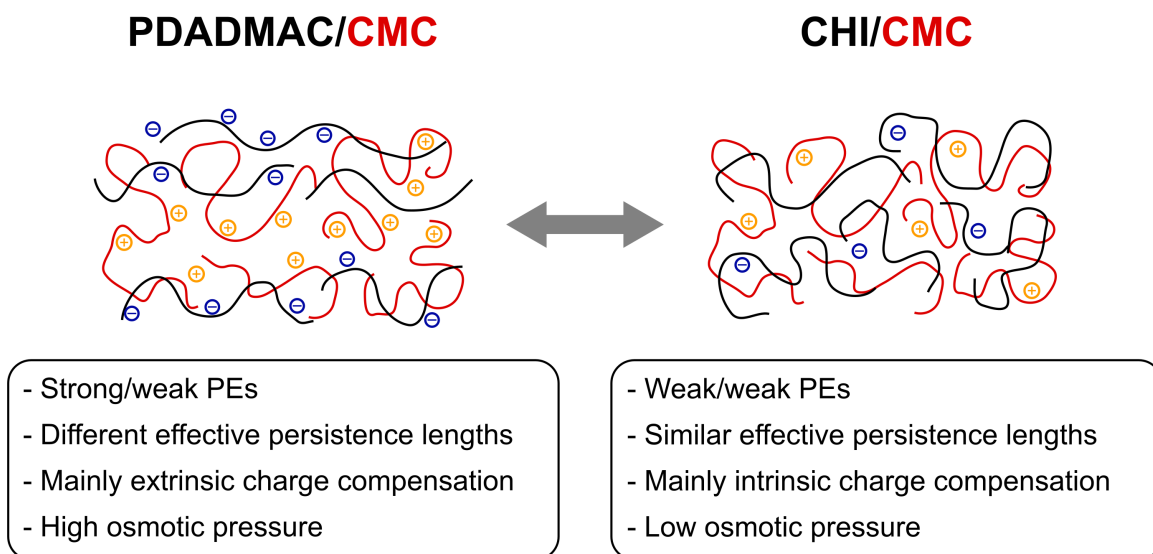


Figure 8: Proposed structures of the PEM systems PDADMAC/CMC and CHI/CMC, resulting from the high charge density of PDADMAC and the high effective persistence length. The polycations are depicted in black, the corresponding negatively charged counter ions in blue. The polyanions are depicted in red, the corresponding positively charged counter ions in orange.

Cellulose model surfaces are used for the study of the functionalization of paper, as it not only enables the broadening of the range of possible analysis methods, but also excludes errors from the randomness and complex structure of the fiber surface. The preparation of PDADMAC/CMC

and CHI/CMC PEMs should allow an extensive study of fiber-polymer interaction. The PDAD-MAC/CMC PEMs are thin and smooth, independent of the NoBL (above a thickness of 50 nm). The smooth film enables the study of the chemical interaction of functional additive with the model surface. On the other hand, the surface of the CHI/CMC PEMs with controlled roughness can mimic the rough surface of a fiber and can be used to study the physical share of the interaction. It is known that the swelling of the fibers during the paper preparation has an influence on the modification and the studied swelling behavior of the PEMs can be used to further study the effect of the integration of the functional additives into the fiber wall on the functionalization.

## Acknowledgement

The authors thank the Deutsche Forschungsgemeinschaft (DFG) under the grant PAK 962-1, sub-project B4 (KL1165/28-1) for the funding of this project.

## Conflict of Interest

The authors have no conflict to declare.

## Author Contributions

Conceptualization, C.L., R.v.K.; formal analysis, C.L., T.T.; investigation, C.L., T.T.; writing—original draft preparation, C.L.; writing—review and editing, C.L., R.G., O.S., R.v.K.; visualization, C.L.; supervision, R.v.K.; project administration, R.v.K.; funding acquisition, R.v.K. All authors have read and agreed to the published version of the manuscript.

## References

- (1) Dufresne, A. *Monomers, Polymers and Composites from Renewable Resources*; Elsevier, 2008; pp 401–418.

- (2) Tavakolian, M.; Jafari, S. M.; van de Ven, T. G. M. A Review on Surface-Functionalized Cellulosic Nanostructures as Biocompatible Antibacterial Materials. *Nano-Micro Letters* **2020**, *12*, 73.
- (3) Tang, R. H.; Liu, L. N.; Zhang, S. F.; He, X. C.; Li, X. J.; Xu, F.; Ni, Y. H.; Li, F. A review on advances in methods for modification of paper supports for use in point-of-care testing. *Microchimica Acta* **2019**, *186*, 521.
- (4) Rinaudo, M. Main properties and current applications of some polysaccharides as biomaterials. *Polymer International* **2008**, *57*, 397–430.
- (5) Dunlop-Jones, N. *Paper Chemistry*; Springer Netherlands: Dordrecht, 1991; pp 76–96.
- (6) Gulsoy, S. K. Effects of cationic starch addition and pulp beating on strength properties of softwood kraft pulp. *Starch - Stärke* **2014**, *66*, 655–659.
- (7) Lindström, T.; Wågberg, L.; Larsson, T. On the nature of joint strength in paper – a review of dry and wet strength resins used in paper manufacturing. *13th Fundamental Research Symposium* **2005**,
- (8) Rojas, J.; Azevedo, E. Functionalization and crosslinking of microcrystalline cellulose in aqueous media: A safe and economic approach. 2011.
- (9) Xu, G. G.; Yang, C. Q.; Deng, Y. Combination of bifunctional aldehydes and poly(vinyl alcohol) as the crosslinking systems to improve paper wet strength. *Journal of Applied Polymer Science* **2004**, *93*, 1673–1680.
- (10) Gunnars, S.; Wågberg, L.; Cohen Stuart, M. A. Model films of cellulose: I. Method development and initial results. *Cellulose* **2002**,
- (11) Kontturi, E.; Tammelin, T.; Österberg, M. Cellulose—model films and the fundamental approach. *Chemical Society Reviews* **2006**,

- (12) Kontturi, E.; Spirk, S. Ultrathin films of cellulose: A materials perspective. 2019.
- (13) Bismarck, A.; Aranberri-Askargorta, I.; Springer, J.; Lampke, T.; Wielage, B.; Stamboulis, A.; Shenderovich, I.; Limbach, H. H. Surface characterization of flax, hemp and cellulose fibers; Surface properties and the water uptake behavior. *Polymer Composites* **2002**,
- (14) Chinga-Carrasco, G. Exploring the multi-scale structure of printing paper - A review of modern technology. *Journal of Microscopy* **2009**,
- (15) Medronho, B.; Romano, A.; Miguel, M. G.; Stigsson, L.; Lindman, B. Rationalizing cellulose (in)solubility: reviewing basic physicochemical aspects and role of hydrophobic interactions. *Cellulose* **2012**, *19*, 581–587.
- (16) Dawsey, T. R.; McCormick, C. L. *Journal of Macromolecular Science, Part C*; 1990; Vol. 30; pp 405–440.
- (17) Kargl, R.; Mohan, T.; Ribitsch, V.; Saake, B.; Puls, J.; Stana-Kleinschek, K. Cellulose thin films from ionic liquid solutions. *Nordic Pulp and Paper Research Journal* **2015**,
- (18) Edgar, C. D.; Gray, D. G. Smooth model cellulose I surfaces from nanocrystal suspensions. *Cellulose* **2003**,
- (19) Aulin, C.; Ahok, S.; Josefsson, P.; Nishino, T.; Hirose, Y.; Österberg, M.; Wågberg, L. Nanoscale cellulose films with different crystallinities and mesostructures - Their surface properties and interaction with water. *Langmuir* **2009**,
- (20) Jahan, M. S.; Noori, A.; Ahsan, L.; Nasima, C. D.; Quaiyyum, M. A. Effects of chitosan as dry and wet strength additive in bamboo and acacia pulp. *IPPTA: Quarterly Journal of Indian Pulp and Paper Technical Association* **2009**,
- (21) Taketa, T. B.; Dos Santos, D. M.; Fiamingo, A.; Vaz, J. M.; Beppu, M. M.; Campana-Filho, S. P.; Cohen, R. E.; Rubner, M. F. Investigation of the Internal Chemical Composition

- of Chitosan-Based LbL Films by Depth-Profiling X-ray Photoelectron Spectroscopy (XPS) Analysis. *Langmuir* **2018**,
- (22) Bataglioli, R. A.; Taketa, T. B.; Neto, J. B.; Lopes, L. M.; Costa, C. A.; Beppu, M. M. Analysis of pH and salt concentration on structural and model-drug delivery properties of polysaccharide-based multilayered films. *Thin Solid Films* **2019**,
- (23) Spera, M. B. M.; Taketa, T. B.; Beppu, M. M. Roughness dynamic in surface growth: Layer-by-layer thin films of carboxymethyl cellulose/chitosan for biomedical applications. *Biointerfaces* **2017**, *12*, 04E401.
- (24) Zhang, S.; Liu, W.; Liang, J.; Li, X.; Liang, W.; He, S.; Zhu, C.; Mao, L. Buildup mechanism of carboxymethyl cellulose and chitosan self-assembled films. *Cellulose* **2013**,
- (25) Löhmann, O.; Zerball, M.; Von Klitzing, R. Water Uptake of Polyelectrolyte Multilayers Including Water Condensation in Voids. *Langmuir* **2018**,
- (26) Lavalle, P.; Picart, C.; Mutterer, J.; Gergely, C.; Reiss, H.; Voegel, J. C.; Senger, B.; Schaaf, P. Modeling the Buildup of Polyelectrolyte Multilayer Films Having Exponential Growth. *Journal of Physical Chemistry B* **2004**,
- (27) Tang, K.; Besseling, N. A. M. Formation of polyelectrolyte multilayers: ionic strengths and growth regimes. *Soft Matter* **2016**, *12*, 1032–1040.
- (28) Volodkin, D.; von Klitzing, R. Competing mechanisms in polyelectrolyte multilayer formation and swelling: Polycation–polyanion pairing vs. polyelectrolyte–ion pairing. *Current Opinion in Colloid & Interface Science* **2014**, *19*, 25–31.
- (29) Kujawa, P.; Moraille, P.; Sanchez, J.; Badia, A.; Winnik, F. M. Effect of Molecular Weight on the Exponential Growth and Morphology of Hyaluronan/Chitosan Multilayers: A Surface Plasmon Resonance Spectroscopy and Atomic Force Microscopy Investigation. *Journal of the American Chemical Society* **2005**, *127*, 9224–9234.

- (30) Abdelkebir, K.; Gaudière, F.; Morin-Grognnet, S.; Coquerel, G.; Labat, B.; Atmani, H.; Ladam, G. Evidence of different growth regimes coexisting within biomimetic Layer-by-Layer films. *Soft Matter* **2011**,
- (31) Porcel, C.; Lavalle, P.; Ball, V.; Decher, G.; Senger, B.; Voegel, J. C.; Schaaf, P. From Exponential to Linear Growth in Polyelectrolyte Multilayers. *Langmuir* **2006**,
- (32) Wang, W.; Xu, Y.; Backes, S.; Li, A.; Micciulla, S.; Kayitmazer, A. B.; Li, L.; Guo, X.; von Klitzing, R. Construction of Compact Polyelectrolyte Multilayers Inspired by Marine Mussel: Effects of Salt Concentration and pH As Observed by QCM-D and AFM. *Langmuir* **2016**, *32*, 3365–3374.
- (33) von Klitzing, R. Internal structure of polyelectrolyte multilayer assemblies. 2006.
- (34) Steitz, R.; Jaeger, W.; von Klitzing, R. Influence of Charge Density and Ionic Strength on the Multilayer Formation of Strong Polyelectrolytes. *Langmuir* **2001**, *17*, 4471–4474.
- (35) Dubas, S. T.; Schlenoff, J. B. Factors Controlling the Growth of Polyelectrolyte Multilayers. *Macromolecules* **1999**, *32*, 8153–8160.
- (36) Garg, A.; Heflin, J. R.; Gibson, H. W.; Davis, R. M. Study of Film Structure and Adsorption Kinetics of Polyelectrolyte Multilayer Films: Effect of pH and Polymer Concentration. *Langmuir* **2008**, *24*, 10887–10894.
- (37) Mermut, O.; Barrett, C. J. Effects of Charge Density and Counterions on the Assembly of Polyelectrolyte Multilayers. *The Journal of Physical Chemistry B* **2003**, *107*, 2525–2530.
- (38) Sui, Z.; Salloum, D.; Schlenoff, J. B. Effect of Molecular Weight on the Construction of Polyelectrolyte Multilayers: Stripping versus Sticking. *Langmuir* **2003**, *19*, 2491–2495.
- (39) Fery, A.; Schöler, B.; Cassagneau, T.; Caruso, F. Nanoporous thin films formed by salt-induced structural changes in multilayers of poly(acrylic acid) and poly(allylamine). *Langmuir* **2001**,



- (40) Lehaf, A. M.; Hariri, H. H.; Schlenoff, J. B. Homogeneity, modulus, and viscoelasticity of polyelectrolyte multilayers by nanoindentation: Refining the buildup mechanism. *Langmuir* **2012**,
- (41) Fenstermaker, C. A.; McCrackin, F. L. Errors arising from surface roughness in ellipsometric measurement of the refractive index of a surface. *Surface Science* **1969**, *16*, 85–96.
- (42) Meier, R.; Ruderer, M. A.; Diethert, A.; Kaune, G.; K"orstgens, V.; Roth, S. V.; M"uller-Buschbaum, P. Influence of Film Thickness on the Phase Separation Mechanism in Ultrathin Conducting Polymer Blend Films. *The Journal of Physical Chemistry B* **2011**, *115*, 2899–2909.
- (43) Ghossoub, Y. E.; Zerball, M.; Fares, H. M.; Ankner, J. F.; von Klitzing, R.; Schlenoff, J. B. Ion distribution in dry polyelectrolyte multilayers: a neutron reflectometry study. *Soft Matter* **2018**, *14*, 1699–1708.
- (44) Wong, J. E.; Rehfeldt, F.; Hänni, P.; Tanaka, M.; von Klitzing, R. Swelling Behavior of Polyelectrolyte Multilayers in Saturated Water Vapor. *Macromolecules* **2004**, *37*, 7285–7289.
- (45) Wang, W.; Xu, Y.; Han, H.; Micciulla, S.; Backes, S.; Li, A.; Xu, J.; Shen, W.; von Klitzing, R.; Guo, X. Odd-even effect during layer-by-layer assembly of polyelectrolytes inspired by marine mussel. *Journal of Polymer Science Part B: Polymer Physics* **2017**, *55*, 245–255.
- (46) Zerball, M.; Laschewsky, A.; von Klitzing, R. Swelling of Polyelectrolyte Multilayers: The Relation Between, Surface and Bulk Characteristics. *The Journal of Physical Chemistry B* **2015**, *119*, 11879–11886.
- (47) Nestler, P.; Block, S.; Helm, C. A. Temperature-Induced Transition from Odd–Even to Even–Odd Effect in Polyelectrolyte Multilayers Due to Interpolyelectrolyte Interactions. *The Journal of Physical Chemistry B* **2012**, *116*, 1234–1243.

- (48) Lavalle, P.; Gergely, C.; Cuisinier, F. J.; Decher, G.; Schaaf, P.; Voegel, J. C.; Picart, C. Comparison of the structure of polyelectrolyte multilayer films exhibiting a linear and an exponential growth regime: An in situ atomic force microscopy study. *Macromolecules* **2002**,